Climate Change Reveals Contrasting Vulnerability: Asymmetric Range Shifts of Two *Dianthus* Species in the Irano-Anatolian Biodiversity Hotspot

Maryam Behroozian*

Herbarium FUMH, Ferdowsi University of Mashhad, Mashhad, Iran. *maryam.behroozian94@gmail.com*

Corresponding author:

E–mail: *maryam.behroozian94@gmail.com*

Address: Herbarium FUMH, Ferdowsi University of Mashhad, Mashhad, Iran

Abstract

The Irano-Anatolian biodiversity hotspot harbors exceptional plant richness and endemism but faces severe threats from climate change. We used MaxEnt-based ecological niche models to evaluate the current and future distributions of two closely related species, *Dianthus floribundus* and *Dianthus szowitsianus*. Models were projected for mid-century (2041–2070) and late-century (2071–2100) under SSP3-7.0 and SSP5-8.5 scenarios. Temperature-related predictors, particularly annual mean temperature (bio1) and temperature seasonality (bio4), were the dominant drivers, yet the species showed markedly different responses to future climates. *D. floribundus*, characterized by a narrow thermal niche, is predicted to undergo severe habitat contraction (up to 60%) and pronounced elevational and latitudinal shifts toward northern high-elevation refugia, consistent with the "escalator to extinction" paradigm for cold-adapted mountain taxa. In contrast, *D. szowitsianus* displayed broader climatic tolerance and ecological plasticity, maintaining most of its core range while expanding into newly suitable habitats, with projected gains exceeding 50%. These asymmetric outcomes highlight the species-specific nature of climate change impacts even among closely related endemics and forecast a decoupling of historical assemblages, with potential consequences for montane community structure and species interactions. Moreover, the reduction of overlap between the two species and the limited representation of persistent habitats within current protected areas underscore the urgent need for forward-looking conservation strategies. Our findings emphasize that conserving montane biodiversity in global hotspots requires species-focused vulnerability assessments, identification of future refugia, and adaptive management frameworks to mitigate differential risks and preserve endemic diversity under climate change.

Keywords: Climate change impacts, Ecological Niche Modeling, Habitat overlap, Projected distribution shifts, Protected areas, closely related species.

Introduction

Biodiversity hotspots are regions of exceptional species richness and endemism that simultaneously face high levels of threat[1,2]. Although they cover a small fraction of the Earth's land surface, they harbor more than half of the world's endemic plants and a large proportion of terrestrial vertebrates, making them global priorities for conservation[3]. The unique and irreplaceable biodiversity within these hotspots is increasingly vulnerable to anthropogenic pressures, particularly land-use change, habitat fragmentation, and global climate change[4,5,6].

Among these critical regions, the Irano-Anatolian biodiversity hotspot represents one of the most floristically rich centers of diversity in western Asia[7,5]. Its complex topography, including the Alborz and Zagros Mountains systems and the Anatolian Plateau, has fostered a wide array of habitats and high levels of endemism[4]. The region's montane ecosystems are particularly important, as they contain a disproportionately high number of endemic taxa that are often restricted to narrow elevational ranges, underscoring their vulnerability to environmental shifts.

Mountain floras are acutely sensitive to climate change. Rising temperatures and altered precipitation regimes are expected to drive upslope and poleward shifts in species distributions, often compressing suitable habitats into smaller,

isolated refugia[8,9]. Alpine and subalpine specialists are especially at risk due to their narrow thermal niches and limited dispersal capacities, with many predicted to face severe range contractions or extinction in the coming decades[10,11]. Recent assessments across the Irano-Anatolian biodiversity hotspot suggest that such pressures may result in dramatic reductions of suitable habitats for many endemic plants, potentially leading to large-scale community restructuring as traditional assemblages disaggregate and species are forced into fragmented climatic refugia[12]. These emerging patterns highlight the urgency of understanding species-specific responses to climate change, since closely related taxa may diverge sharply in their ecological trajectories depending on their niche breadth and environmental tolerances. To this end, we selected two closely related *Dianthus* species in the Irano-Anatolian biodiversity hotspot to investigate their species-specific responses to climate change in this region.

The genus *Dianthus* is well represented in the Irano-Anatolian biodiversity hotspot, particularly across calcareous and montane steppe systems[4,6]. *Dianthus floribundus* Boiss. is an Irano-Turanian element recorded from eastern Anatolia, Armenia, and Iran, where it occupies open steppe and rocky slopes, frequently on limestone[13,14,15]. Many populations occur within calcareous steppe mosaics of the Central and Eastern Anatolian plateau, typically on rocky limestone slopes and open steppe above ~1,000 m. By contrast, *Dianthus szowitsianus* Boiss. is primarily reported from Iran, with verified records along the Central Alborz near Tehran and in north-western Iran, including the Sabalan massif. *D. szowitsianus* is considered an endemic species of Iran according to recent floristic treatments and global plant databases[4,14,15,16,17]. [14](1988) and[15](2023) place *D. floribundus* and *D. szowitsianus* in close taxonomic proximity due to their morphological similarity, despite their distinct ecological and geographical ranges. The geology of its Iranian range spans both carbonate and volcanic substrates: the Alborz contains extensive Jurassic–Eocene limestones as well as volcanic–volcaniclastic sequences (e.g., the Karaj Formation) and Quaternary volcanic cones (e.g., Damavand), while Sabalan is an andesitic–dacitic stratovolcano[18,19]. This distribution indicates that *D. szowitsianus* can persist across contrasting edaphic conditions within the hotspot. Taken together, the occurrence of *D. floribundus* in calcareous Anatolian steppe and *D. szowitsianus* on Iranian montane slopes underlain by both carbonate and volcanic lithologies provides a compelling system for testing how climate-driven distributional shifts interact with edaphic constraints in a mountainous biodiversity hotspot.

Ecological niche modeling (ENM) provides a powerful framework for investigating these dynamics by linking occurrence records with environmental predictors to identify key climatic drivers and forecast potential distributional changes under future scenarios[20,21,22]. MaxEnt-based models, in particular, are well-suited for this task due to their ability to handle presence-only data, which is often the only type available for rare or endemic species[23]. These models are invaluable in biodiversity hotspots for identifying potential refugia, anticipating range contractions or expansions, and guiding proactive conservation strategies in the face of environmental uncertainty[24,25].

Here, we use ENMs to investigate the current and projected distributions of *D. floribundus* and *D. szowitsianus* in the Irano-Anatolian biodiversity hotspot. We specifically aim to: (1) Identify the key climatic variables shaping their distributions to assess each variable's contribution to explaining species occurrence; (2) Evaluate how their potential ranges may shift under mid-century (2041–2070) and late-century (2071–2100) climate scenarios, and quantify both elevational and spatial displacements; and (3) Assess the extent of suitable habitat within current protected areas to provide direct implications for the conservation of montane plant diversity in the region. Our study provides an

ecological niche modeling framework for understanding the divergent responses of closely related species to climate change within a critical biodiversity hotspot. By comparing the vulnerabilities of two congeneric species, we provide insights into potential differences in their climatic niche responses under future climate change scenarios. These findings also underscore the need for tailored conservation strategies and have significant implications for preserving montane plant diversity in the Irano-Anatolian biodiversity hotspot.

Materials and Methods

- *Occurrence data collection*

I used occurrence data for *D. floribundus* and *D. szowitsianus* from different sources, in the form of herbarium specimens in the collections of Herbarium of Research Institute of Forests and Rangelands (TARI). Additional records were sourced from key floristic references, including *Flora Iranica* (Rechinger 1988), the *Flora of Iran*[15], and an old literature of *Dianthus* species of Iran[26]. I also checked the Global Biodiversity Information Facility (GBIF; http://www.gbif.org/), Virtual Herbaria (https://jacq.org/); JACQ (https://jacq.org/), and SpeciesLink (http://splink.cria.org.br/). All occurrence data were compiled using Microsoft Excel and saved in CSV (.csv) format for subsequent analysis.

All records were visualized and checked in ArcGIS 3.16 to assess geospatial accuracy and detect outliers. Erroneous records (outside known ranges, missing or zero coordinates, or >1 km uncertainty) were removed. To reduce spatial autocorrelation and sampling bias, especially in heterogeneous regions, I applied spatial thinning with a 1.1 km filter using the *spThin* R package[27], following ecological reasoning and prior studies[28,29]. In total, 53 and 189 records were compiled for *D. szowitsianus* and *D. floribundus*. After filtering, 41 and 173 unique points remained, respectively (Figure 1a). Occurrence data for each species were randomly partitioned into two equal subsets, with 50% used for model calibration and 50% for evaluation (Figure 1c, d). Although a 75%–25% partition is commonly recommended in species distribution modeling studies[23,30,31], we used a balanced partition to maintain a sufficiently large and independent dataset for model evaluation, particularly given the moderate sample sizes available. In addition to this partitioning scheme, candidate models were evaluated using partial ROC tests, omission rates, and AICc values, following commonly recommended procedures for ecological niche model calibration and model selection[21,32,33]. This multi-criteria evaluation framework reduces dependence on a single training–testing split and provides a more robust assessment of model performance.

- *Environmental data*

Climatic data for both present and future conditions were obtained from CHELSA version 2.1 (Climatologies at High Resolution for Earth's Land Surface[34,35], which provides high-resolution (~1 km, 30 arc-seconds) temperature and precipitation data essential for ecological modeling. These variables, widely used in ecological niche modeling (ENM), were downloaded from the EnviDat data portal (https://doi.org/10.16904/envidat.228). The projections included the current climate (1981–2010) and two future periods (mid-century; 2041-2070) and (late-century; 2071-2100) under two Shared Socioeconomic Pathway (SSP) scenarios: SSP3-7.0 (moderate emissions) and SSP5-8.5 (high emissions). Four Global Circulation Models (GCMs), including GFDL-ESM4, IPSL-CM6A-LR, MPI-ESM1-2HR,

UKESM1-0-LL of CMIP6 (Coupled Model Intercomparison Project Phase 6), were selected for this study (Table S1)[36,37,38].

I removed variables mean temperature of wettest quarter (bio8), mean temperature of driest quarter (bio9), precipitation of warmest quarter (bio18), and precipitation of coldest quarter (bio19) from all of the analyses because of known spatial artifacts[39]. Two-step procedures were used to select subsets of the remaining 15 bioclimatic variables. To identify the most important bioclimatic variables influencing the distribution of the target species, we calculated Variable Importance in Projection (VIP) scores based on a Partial Least Squares (PLS) regression model. VIP scores quantify the contribution of each variable in explaining species occurrence (Table S2). I also conducted Pearson correlation analysis to examine multicollinearity among variables and excluded highly correlated variables ($r > 0.8$). Based on the preliminary analyses, seven bioclimatic variables were identified as important for *D. floribundus* (bio1: annual mean temperature; bio2: mean diurnal range; bio3: isothermality; bio4: temperature seasonality; bio13: precipitation of the wettest month; bio14: precipitation of the driest month; and bio15: precipitation seasonality). For *D. szowitsianus*, six key variables were selected (bio3: isothermality; bio4: temperature seasonality; bio6: minimum temperature of the coldest month; bio7: temperature annual range; bio12: annual precipitation; and bio15: precipitation seasonality). To further refine the predictors, a jackknife procedure was applied by sequentially removing the variable with the lowest independent contribution. This process yielded four optimized predictor sets comprising 6, 5, 4, and 3 variables, which were subsequently used in the modeling for both species.

- *Calibration and projection areas*

Calibration areas (**M**) were defined based on climatic accessibility inferred from present and past climate dynamics using dispersal simulations implemented in the *grinnell* package[40,41,42] (Figure 1c, d). The calibration area refers to the geographic region considered accessible to the species over relevant time periods, within which environmental conditions are used to calibrate the ecological niche model. This concept corresponds to the accessible area ("**M**") in the BAM framework. Simulations incorporated occurrence records and 19 bioclimatic variables at 30′ resolution. Unlike the ecological niche models, the simulation procedure used the complete climatic dataset to represent the overall climatic space of the study area. Each simulation was run for 100 time steps with 10 replicates using a normal dispersal kernel, and the kernel standard deviation (kernel spread) was varied between 2 and 17 to explore alternative dispersal scenarios. Replicates were averaged and binarized to estimate **M**, which was then used to mask climatic data, restricting calibration to areas species could plausibly access.

Although model calibration was performed within the species-specific accessible area (**M**), spatial projections were extended to the entire study region to identify climatically suitable areas beyond the currently occupied range. Model projections covered western Asia (Figure 1a), Iran, Turkmenistan, Turkey, Armenia, Georgia, Azerbaijan, Syria, Iraq, Lebanon, Israel, and Jordan, broadly overlapping the Irano-Anatolian biodiversity hotspot. As my goal was to assess climate change impacts on two *Dianthus* species in this hotspot, predictive maps and other analyses were limited to this region. Current and future climatic layers were further masked to **M** and the broader Irano-Anatolian biodiversity hotspot region using ArcGIS 10.3.1. Data on the extent of protected areas were compiled from the World Database on Protected Areas (www.protectedplanet.net).

- *Ecological niche models*

I modeled the potential distributions of both species using a Maxent-based approach implemented in the *kuenm* R package[33]. Maxent is well-suited for presence-only, small-sample datasets (notably *D. szowitsianus*), and *kuenm* enables systematic tuning of model complexity[23,33]. Because the number of occurrence records for one species was relatively limited, model calibration and evaluation followed recommended practices for ecological niche modeling with small datasets, including the use of multiple model evaluation criteria to reduce the risk of overfitting[43]. Modeling was conducted with two approaches to account for the small sample size of *D. szowitsianus* versus the larger dataset of *D. floribundus*. For *D. floribundus*, I generated candidate models using four groupings of seven environmental variables, all 29 combinations of Maxent feature types (linear = l, quadratic = q, product = p, threshold = t, and hinge = h), and 10 regularization multiplier (RM) values (0.25, 0.5, 0.75, 1, 1.25, 1.5, 1.75, 2, 3, 4). For *D. szowitsianus*, I tested 11 RM values (0.1, 0.25, 0.5, 0.75, 1.25, 1.5, 1.75, 2, 3, 4, 5) and five feature class combinations (l, lq, lqp, lqpt, lqpth), emphasizing simpler classes to reduce overfitting[32].

Model performance was evaluated using three criteria: statistical significance (partial ROC, $P \leq 0.05$[44]), omission error (<0.05[45]), and minimal complexity (ΔAICc < 2[46]). Models meeting all thresholds were selected for final predictions.

Final models were built with selected parameters, 10 bootstrap replicates, logistic output, and 10,000 background points. This number corresponds to the commonly used default setting in MaxEnt and is generally sufficient to represent the environmental space of the study region while maintaining computational efficiency[47]. Projections were made across the entire study area under current conditions and ten future climate datasets[32,48]. Transferability was assessed with three extrapolation scenarios during model projection: free extrapolation (E), where the model freely predicts suitability in environmental conditions outside the calibration range; clamping (EC), where predictions are constrained to the range of environmental conditions observed during model calibration; and no extrapolation (NE), where predictions are restricted to environments within the calibration range. These approaches are commonly used to evaluate the effects of model extrapolation when projecting ecological niche models[21,33]. Present conditions were summarized as the median across replicates; uncertainty was the range of medians across GCMs for SSP3-7.0 and SSP5-8.5. Future projections used the median of replicate medians across four GCMs for 2041–2070 and 2071–2100, with ranges indicating uncertainty[44]. Replicates were thresholded to binary maps using an omission error threshold of E = 5%, meaning that up to 5% of occurrence records were allowed to be omitted when converting continuous suitability predictions to binary maps. This approach accounts for potential uncertainty in occurrence data and is commonly used in ecological niche modeling[21,49]. To reduce prediction uncertainty, binary maps were filtered in *terra*: uncertainty rasters were resampled, the 90th percentile of values was used as a threshold, and high-uncertainty cells were masked, producing strictly binary outputs (0 = unsuitable/high uncertainty, 1 = suitable/low uncertainty)[50]. Finally, distributional changes across GCMs for SSP3-7.0 and SSP5-8.5 (2041–2070, 2071–2100) were categorized as Unsuitable, Gained, Lost, or Suitable[51]. Analyses were conducted in R version 4.0.0[52] and ArcGIS 10.3.1.

- *Range shift and overlap metrics*

To evaluate the spatial and elevational patterns of climatic niche suitability for the two *Dianthus* species under climate change, ecological niche model outputs were analyzed under both current and projected future climate conditions. Habitat suitability maps were generated for the present and for two future scenarios (SSP3-7.0 and SSP5-8.5) for mid-century (2041–2070) and late-century (2071–2100). To ensure comparability, all raster layers were standardized to a common spatial resolution of 30 arc-seconds (~1 km) to ensure consistency among environmental predictors. Elevational patterns were assessed using a digital elevation model (DEM), which was used to calculate suitability-weighted mean elevation from the predicted suitability maps in order to quantify elevational shifts between current and future projections. Distributional dynamics were quantified by calculating suitability-weighted centroids for each species in both time periods, with geographic shifts expressed as centroid displacement (km)[53]. Elevational shifts were estimated as changes in suitability-weighted mean elevation between current and future projections. Specifically, elevation-weighted habitat suitability was calculated by weighting the elevation value of each grid cell by its corresponding habitat suitability score and then computing the weighted mean elevation. This approach emphasizes areas of higher suitability when estimating the elevational distribution of each species[8].

Binary habitat maps (presence/absence) were derived from continuous suitability layers to assess spatial overlap between species. Each grid cell was classified as unsuitable, suitable for only one species, or suitable for both (overlap areas). I further overlaid these maps with the boundaries of protected areas to quantify the extent of suitable habitats under conservation coverage. All analyses and visualizations were conducted in R, using packages including *raster* version 3.6-32[54]*, terra* version 1.8-54[55], *sf* version 1.0-21[56], and *ggplot2* version 3.5.2[57].

Results

- *Variables' importance and the response curves*

Percent contribution and permutation importance of environmental variables revealed that bio1 (annual mean temperature) and bio4 (temperature seasonality) had the highest contributions, with values of 30.2% and 40.3% for *D. floribundus* and *D. szowitsianus*, respectively. For *D. floribundus*, bio4 (26.7%) and bio3 (isothermality, %) (26.3%) followed, together accounting for 83.2% of the model. In the case of *D. szowitsianus*, bio3 (25.9%) and bio12 (annual precipitation, mm) (21.0%) were the next most important variables, together explaining 87.1% of the model (Table S3).

The response curves for *D. floribundus* indicated that bio1 (°C) showed the highest probability of occurrence approximately between 4 and 15 °C, after which suitability declined markedly at higher temperatures. Bio4 exhibited a continuous increasing trend, with higher temperature seasonality values corresponding to greater predicted suitability. For bio3, the species reached maximum suitability at approximately 28–30%, with a clear decrease at both lower and higher values (Figure 2). In contrast, the response curves for *D. szowitsianus* indicated that bio4 has a strong positive relationship with suitability, with probabilities increasing steadily from around 8000 to a maximum near 12,000. Bio3 showed the highest suitability at lower values (~1.5–2.0%) and declined progressively with increasing values, approaching minimal levels beyond 3.5%. Bio12 exhibited a unimodal relationship, with suitability peaking around 6000 mm and declining sharply at both lower and higher precipitation levels (Figure 2).

- *The model evaluation*

A total of 1,160 candidate Maxent models were generated and evaluated for *D. floribundus* using combinations of 29 feature classes, 10 regularization multipliers, and four environmental datasets. Of these, 1,084 models performed significantly better than random expectations according to the partial ROC test ($P < 0.001$; Table S4). Among the models meeting the statistical significance and omission rate criteria, several models showed similar support according to AICc ($\Delta AICc \leq 2$). From this subset of competing models, a single representative model was selected following the *kuenm* model selection workflow. This best-performing model incorporated three feature classes (linear, product, and threshold), a regularization multiplier of 1.75, and six climatic variables from Set 2 (bio1, bio3, bio4, bio13, bio14, and bio15; Table S4).

For *D. szowitsianus*, 220 candidate models were created by testing combinations of five feature class settings, 11 regularization multipliers, and four environmental datasets defined through the jackknife procedure. Among these, 210 models showed significantly higher predictive performance than random expectations (partial ROC, $P < 0.05$). A subset of models also satisfied the model complexity criterion ($\Delta AICc \leq 2$). From these competing models, one representative model was selected following the *kuenm* model selection procedure. This optimal model employed linear, product, and quadratic feature classes, a regularization multiplier of 0.25, and a five-variable climate set (bio3, bio4, bio7, bio12, and bio15; Table S4). These final models were subsequently used for all projections.

- *Predicted current and future potential distribution patterns*

Under current climatic conditions, the potential distribution of *D. floribundus* spanned highly suitable areas within the Irano-Anatolian biodiversity hotspot. These regions included the central Alborz and northern Zagros Mountains in Iran, the Azerbaijan Plateau, the Hakkari Mountains in Turkey, and the Armenian Highlands. Unsuitability was notably high at the lower latitudes of the Zagros Mountains. While high uncertainty was detected in parts of southern Iran and Turkmenistan, most highly suitable regions, such as the northern Zagros Mountains, the Azerbaijan Plateau, and the Armenian highlands, showed low associated uncertainty. In contrast, *D. szowitsianus* exhibited a more restricted distribution, with suitable habitats confined to smaller portions of the hotspot. High suitability was concentrated in the Hakkari Mountains (Turkey), the central Alborz and Zagros Mountains (Iran), and northern Turkmenistan. Unlike *D. floribundus*, unsuitability for *D. szowitsianus* was predicted in both high- and low-latitude ranges. These predicted suitable areas should be interpreted as potential climatic suitability rather than confirmed occurrence, as ecological niche models estimate the fundamental climatic niche and may identify climatically suitable regions that remain unoccupied due to dispersal limitation, historical biogeographic constraints, or other ecological factors not included in the model. High prediction uncertainty was observed only in the southern Zagros Mountains of Iran (Figure 3).

I projected suitable habitats for both species under SSP3-7.0 and SSP5-8.5 scenarios for the mid-century (2041–2070) and late-century (2071–2100). Future range projections for *D. floribundus* revealed a distributional pattern largely consistent with its current range in the hotspot during the mid-century under both scenarios (Figures 4, S1). High suitability was predicted in the northern, high-latitude parts of the region with relatively low uncertainty, while high unsuitability was observed at lower latitudes. In the late-century, projections indicated a significant reduction in highly

suitable areas, which became increasingly concentrated in the northern parts of the region. This resulted in a large area of low suitability and unsuitability in lower-latitude ranges, including most of the Zagros Mountains and the Azerbaijan Plateau (Figures 4, S1). In contrast, models for *D. szowitsianus* under both scenarios predicted an expansion of suitable areas compared to current conditions in both the mid- and late-century. High suitability was forecasted to shift to more southern parts of the hotspot, including areas south of the Hakkari Mountains (Turkey) and parts of the southern and central Zagros Mountains. Additionally, my models projected high suitability in the central Alborz Mountains and a small part of the hotspot region in Turkmenistan. High uncertainty was observed predominantly in the southern Zagros Mountains (Figures 4, S1).

Figure 5a for *D. floribundus* showed a pronounced contraction of high-suitability areas toward higher latitudes by the late century (2071–2100). The total suitable area was projected to decline from 404,222.8 km² (44.4% of the hotspot) under current conditions to 209,389.1 km² (23.0%) under the SSP5-8.5 scenario, representing a severe contraction of nearly 60% (Table 1). During the mid-century, suitable areas were larger, with 405,983.2 km² (44.6%) under SSP3-7.0 and 371,798.3 km² (40.9%) under SSP5-8.5. This period showed relatively higher habitat persistence (77.1% and 72.4%, respectively) compared to late-century scenarios. By the late-century under SSP5-8.5, range loss reached 242,168.4 km², and habitat persistence declined significantly to only 40.1%. Habitat expansion remained minimal across all scenarios, staying at or below 23.3% (Table 1). Within protected areas (Figure 5b), the suitable habitat for *D. floribundus*, which currently covers 22,155.4 km², was projected to decline steadily. Suitability was forecasted to decrease to 9,389.5 km² under SSP5-8.5 (2041–2070) and further to 5,566.1 km² under SSP5-8.5 (2071–2100). Habitat expansion was consistently low (3,029–3,722 km²), whereas habitat contraction progressively increased (5,836–10,567 km²). Stable habitat also decreased from 10,297.2 km² to 5,566.1 km² across the scenarios.

In contrast, *D. szowitsianus* was projected to experience substantial habitat expansion and spatial shifts (Figure 5a). Its distribution was predicted to increase from 273,931.1 km² (30.1%) under current conditions to a maximum of 587,341.9 km² (64.6%) by the late-century under SSP3-7.0, corresponding to a 56.4% expansion (Table 1). New habitats were expected to account for more than 47% of the suitable range in all scenarios, while habitat contraction was projected to remain consistently low (<8%). The persistence of current habitat was exceptionally high, exceeding 92% across all scenarios. Within protected areas, a relatively high proportion of climatically suitable habitat remained stable (>36%), suggesting that these areas may continue to provide suitable climatic conditions for the species under future scenarios (Figure 5b; Table S4). The projected gains in suitable habitat (up to 22.5% under SSP3-7.0 by late-century) far outweigh the minimal losses (<1%) (Figure 5b, Table S5).

- *Range shift and overlap metrics assessment*
  - *Projected distribution shifts*

The elevation-weighted density of habitat suitability for *D. floribundus* under current conditions peaked around 2000–2200 m. In future scenarios, the distribution shifted upward, with peaks at 1800-2000 m under SSP3-7.0 and 1800-2000 m under SSP5-8.5 for 2041–2070. By 2071–2100, the peaks were observed at 1800-2000 m under SSP3-7.0 and 1800-2000 m under SSP5-8.5. The overall density values decreased through time, with the strongest reduction under SSP5-8.5 in the late-century period. For *D. szowitsianus*, the current suitability peak was located at 1000–1500 m. In

future projections, the peaks shifted moderately upward, reaching 1000–2000 m under SSP3-7.0 and SSP5-8.5 in 2041–2070. In 2071–2100, the peaks were located at 1000–2000 m under SSP3-7.0 and 1000–2000 m under SSP5-8.5. Unlike *D. floribundus*, the density values of *D. szowitsianus* increased in future scenarios, particularly under SSP3-7.0 at the end of the century (Figure 6). Globally, *D. floribundus* shortens in low areas and widens in high areas while *D. szowitsianus* contracts at both extremes and expands at 1500-2100. Projected centroid shifts revealed larger displacements for *D. floribundus* compared to *D. szowitsianus*. In *D. floribundus*, centroid movements ranged from 46.5 km under SSP3-7.0 (2041–2070) to 99.6 km under SSP3-7.0 (2071–2100). Elevational shifts were consistently upward, ranging from 63.1 m (SSP3-7.0, 2041–2070) to 118.2 m (SSP5-8.5, 2071–2100). Latitudinal changes reached up to 0.62°, while longitudinal shifts extended to –0.81°. The bearing of centroid movement varied from 310.8° under SSP3-7.0 (2041–2070) to 332.8° under SSP5-8.5 (2071–2100), indicating a predominantly northwestern trajectory (Table 2; Figures S2, S3).

For *D. szowitsianus*, centroid displacements were smaller, ranging between 26.2 km (SSP3-7.0, 2041–2070) and 37.9 km (SSP3-7.0, 2071–2100). Elevational changes varied from –4.7 m under SSP5-8.5 (2041–2070) to +45.4 m under SSP5-8.5 (2071–2100). Latitudinal shifts ranged from –0.21° to +0.04°, while longitudinal displacements reached up to –0.42°. The bearing values ranged from 206.9° (SSP3-7.0, 2041–2070) to 278.4° (SSP5-8.5, 2071–2100), reflecting predominantly westward to southwestward trajectories (Table 2; Figures S2, S3).

In Figure S3, centroid and elevation shifts highlighted a clear contrast between the two species. For *D. floribundus*, centroid shifts increased from 46.5 km (SSP3-7.0, 2041–2070) to 99.6 km (SSP3-7.0, 2071–2100), with elevation rising from 63.1 m to 118.2 m across scenarios. In contrast, *D. szowitsianus* showed much smaller centroid shifts, between 26.2 km and 37.9 km, with elevation changes ranging from –4.7 m to +45.4 m. The comparative patterns demonstrated stronger and more consistent spatial and elevational displacements for *D. floribundus* across all scenarios, whereas *D. szowitsianus* exhibited limited shifts with minimal elevational responses.

- *Habitat overlap and protected area effectiveness*

The predicted spatial overlap of *D. floribundus* and *D. szowitsianus* showed distinct patterns across future scenarios in relation to the protected areas of the Irano-Anatolian biodiversity hotspot. Under current conditions, the overlap was extensive across the central and northern parts of the hotspot. In future projections, both the extent and position of overlap shifted depending on the scenario and time horizon. Overall, the models consistently projected a marked contraction of overlap by the late century (2071–2100), driven by the expansion of *D. szowitsianus* into new areas and the concurrent retreat of *D. floribundus*, particularly in the southern portion of the hotspot (Figure 7).

Numerical assessments confirmed these spatial changes (Table 3). Under SSP3-7.0 for 2041–2070, *D. floribundus* covered 184,053.3 km², of which 4,815.4 km² (2.61%) occurred inside protected areas. *D. szowitsianus* occupied 308,699.0 km², with 11,671.7 km² (3.78%) inside protected areas. The overlap between the two species was 227,183.0 km², of which 9,122.1 km² (4.01%) was located within protected areas. Under SSP5-8.5 for 2041–2070, the area of *D. floribundus* was 193,798.6 km², with 4,968.4 km² (2.56%) inside protected areas, while *D. szowitsianus* covered 315,374.5 km², with 12,694.3 km² (4.02%) in protected areas. Their overlap decreased to 182,590.1 km², with 7,824.5 km² (4.28%) within protected areas.

By late-century (2071–2100), the trends continued. Under SSP3-7.0, *D. floribundus* contracted to 120,244.9 km², with 3,863.0 km² (3.21%) inside protected areas. *D. szowitsianus* expanded to 404,765.6 km², with 14,589.1 km² (3.60%) in protected areas. The overlap was 188,217.7 km², of which 7,614.7 km² (4.04%) occurred inside protected areas. Under SSP5-8.5 for 2071–2100, *D. floribundus* further contracted to 106,395.2 km², with 3,845.3 km² (3.61%) in protected areas. *D. szowitsianus* expanded to 463,376.2 km², with 17,290.4 km² (3.73%) inside protected areas. The overlap was reduced to 105,449.1 km², of which 4,682.1 km² (4.44%) was located in protected areas.

Discussion

This study investigates the potential geographic distribution of two *Dianthus* species in the Irano-Anatolian region under current and projected future climate conditions. Our ecological niche models found that temperature-related variables are the most influential factors shaping the distributions of both *D. floribundus* and *D. szowitsianus*. Crucially, however, the results highlight a clear divergence in their climatic niches[20,21].

- *The mechanisms leading to the different responses to climate changes*

For *D. floribundus*, annual mean temperature (bio1) and temperature seasonality (bio4) were the dominant predictors, collectively explaining a high proportion of the model's performance. The response curves indicate an optimal temperature range, approximately 4–15 C°, followed by a sharp decline in suitability at higher values. This strong sensitivity to temperature underscores the species' vulnerability to global warming and is consistent with its projected habitat contraction[10,58]. The additional importance of isothermality (bio3) suggests that *D. floribundus* is particularly adapted to environments characterized by relatively stable daily and seasonal thermal regimes, further reinforcing its ecological specialization. In contrast, while temperature seasonality (bio4) was also the most influential predictor for *D. szowitsianus*, its distribution was further shaped by a broader set of variables, notably isothermality (bio3) and annual precipitation (bio12). The response curves indicate that habitat suitability for this species increases with higher temperature seasonality but peaks at lower isothermality values, reflecting a clear preference for environments with more pronounced temperature variability[53]. Similar patterns have been reported in previous studies of montane and alpine plant species[59,60,61]. Moreover, the unimodal relationship with annual precipitation, with an optimum around intermediate rainfall levels, points to a critical climatic dependence on balanced moisture conditions and a sensitivity to both excessively dry and overly wet environments. Comparable responses to precipitation gradients have also been documented in previous ecological studies[62].

These findings show that even within the same genus and biogeographic region, endemic species may exhibit markedly different responses to climate change due to their distinct ecological requirements. *D. floribundus* exemplifies a narrowly adapted species with a restricted thermal niche within the climatic space represented in our models, making it highly vulnerable to habitat loss under warming scenarios. By contrast, *D. szowitsianus* displays greater ecological plasticity, responding to multiple climatic factors that may facilitate its persistence and even range expansion into newly suitable habitats. Similar patterns of contrasting climatic responses among closely related species have been reported in previous studies[12]. Such divergent outcomes are consistent with broader evidence from the Irano-Anatolian biodiversity hotspot, where many high-elevation endemics are constrained by narrow thermal

niches and strong seasonal variability. This vulnerability is often attributed to climatic niche conservatism, the tendency of alpine plants to retain ancestral climatic preferences despite ongoing environmental change[7,8,63]. In this context, *D. floribundus* is likely to suffer range contraction, whereas *D. szowitsianus* may benefit from its broader climatic tolerance. These contrasting responses underscore the species-specific nature of climate change impacts and highlight the urgent need for conservation strategies tailored to the ecological characteristics and vulnerabilities of individual taxa.

From a mechanistic perspective, the contrasting climatic responses of the two species may be linked to underlying physiological and functional traits that determine their ecological adaptations. Species constrained by mean temperature and low thermal variability, such as *D. floribundus*, are typically characterized by narrow thermal tolerance and limited phenotypic plasticity, traits common in cold-adapted montane plants[64,65]. In contrast, species responding to temperature seasonality and precipitation gradients, such as *D. szowitsianus*, are more likely to exhibit broader physiological tolerances and greater flexibility in water-use and environmental responses[66,67]. Functional traits including leaf morphology, stomatal regulation, and phenology play a key role in mediating responses to temperature and moisture variability[68]. Additionally, adaptation to specific substrates such as calcareous rocky habitats may further constrain resource acquisition and reinforce niche differentiation. Similar links between climatic niche differentiation and plant functional traits have been reported in other montane species, where variation in drought tolerance, thermal sensitivity, and plasticity drives species-specific responses to climate change[64,67].

Our projections suggest sharply contrasting responses of *D. floribundus* and *D. szowitsianus* niche to future climate change within the Irano-Anatolian biodiversity hotspot, underlining the highly species-specific nature of climate impacts in montane ecosystems. While *D. floribundus* is consistently predicted to lose large parts of its suitable range, particularly across the southern Zagros Mountains and the Azerbaijan Plateau, with persistence limited to northern and higher-elevation refugia, *D. szowitsianus* is projected to maintain most of its currently suitable climatic areas and show an increase in climatically suitable habitats in the central Zagros and Alborz Mountains, as well as areas south of the Hakkari Mountains. These divergent trajectories illustrate how closely related taxa may follow opposite fates when exposed to the same climatic pressures, a phenomenon also reported for other Irano-Turanian species such as *Dianthus polylepis*, which exhibits strong range contractions alongside the emergence of novel suitable niches under future climates[59]. *D. floribundus* is projected to retreat from lower-latitude and lower-elevation sectors of the Irano-Anatolian biodiversity hotspot and to persist mainly in cooler, northerly, and higher-elevation refugia, whereas *D. szowitsianus* maintains most of its core distribution and expands into newly suitable portions of the hotspot. The spatially explicit suitability maps, centroid vectors, and elevation-weighted density analyses collectively show that *D. floribundus* undergoes substantial upslope and poleward displacement while *D. szowitsianus* exhibits modest elevational change but notable range gains and high persistence (see Figures 5, 6, S2, S3, and Tables 2, 3). Such divergent outcomes are biologically plausible because they reflect differences in climatic drivers and niche sensitivities: our variable-importance outputs indicate that *D. floribundus* is strongly structured by mean temperature and precipitation seasonality, whereas *D. szowitsianus* responds primarily to temperature seasonality, differences that readily translate into contrasting capacities to tolerate warming and altered precipitation regimes (see Figure 2, Table S3). These species-level contrasts mirror prior work on Irano-Turanian plants: modeling of *Dianthus polylepis*

likewise found upward shifts and contractions of core climatic suitability, demonstrating that closely related montane species can respond differently depending on their climatic niche and dispersal context[59]. Although *D. szowitsianus* exhibits greater climatic breadth or plasticity, its observed occurrences remain fewer than those of *D. floribundus*. This discrepancy likely results from dispersal limitations, historical biogeographic constraints, and specific habitat requirements (e.g., calcareous rocky steppe) that restrict its realized distribution. Non-climatic factors such as competition, biotic interactions, and local disturbances may also play a role. Additionally, uneven sampling and limited field surveys could underestimate its true occurrence. Therefore, while our models capture the fundamental climatic niche, the realized distribution of *D. szowitsianus* is constrained by a combination of ecological and historical factors.

- *The cascading consequences for ecological networks by the decoupling of ranges of similar species*

The elevational dynamics we document for *D. floribundus*, characterized by progressive upward movement of suitability peaks and larger centroid displacements, are characteristic of the "escalator to extinction" paradigm for cold-adapted mountain taxa. Warming compresses suitable thermal belts into ever smaller and more fragmented high-elevation patches, increasing extinction risk[11,61,69]. The accompanying loss of suitability at lower elevations and in southern portions of the hotspot underscores how topography and latitude jointly constrain available refugia for cold specialists. By contrast, the limited upslope response and net increase in suitability for *D. szowitsianus* suggest greater climatic breadth or plasticity, enabling colonization of emerging mid-elevation niches; this pattern accords with regional findings that some montane endemics, given appropriate traits and dispersal pathways, may expand even as others contract[24,70,71,72].

Viewed in the hotspot context, these species trajectories acquire additional conservation significance. The Irano-Anatolian region concentrates a large fraction of Iran's endemics in its mountain ranges (Zagros and Alborz Mountains, Azerbaijan Plateau, and Armenian Highlands)[4], and recent hotspot-scale modeling indicates that endemic plant diversity here is broadly vulnerable to future climate change with potential for large-scale community restructuring even where species are currently abundant[12]. Our finding that *D. floribundus* is likely to become increasingly confined to northern/high-elevation refugia exemplifies this hotspot-wide sensitivity, while the expansion of *D. szowitsianus* illustrates that some taxa may temporarily benefit from shifting climates; importantly, expansion is not equivalent to long-term security, because biotic interactions, dispersal limitations, and land-use change can prevent realized range occupation[73,74].

The projected decoupling of ranges, a marked reduction in spatial overlap between the two species over time, implies that longstanding local assemblages could disaggregate, with cascading consequences for ecological networks. Reduced co-occurrence may alter competition dynamics, pollinator sharing, and facilitative microhabitat relationships that are often crucial in montane communities. For instance, retreat of *D. floribundus* from lower elevations could reduce floral resources for specialized pollinators, while loss of cushion-forming plants may decrease soil stability and microhabitat availability for other mountain specialists[11,75]. This argument is reinforced by recent regional studies of cushion and other structurally important mountain lifeforms: research in adjacent provinces (e.g., Khorassan–Kopet Dagh) shows that cushion species and other mountain specialists are predicted to shift upslope and lose large parts of their suitable area, and because cushions function as ecological engineers, their decline can cascade through

ecosystems by reducing soil stability, microhabitat availability, and floral resources for pollinators[60]. Such changes not only affect species interactions but also ecosystem processes like nutrient cycling and habitat complexity.

Overlaying projected suitability onto existing protected-area boundaries highlights a further concern: the long-term persistence areas for the more vulnerable species frequently lie at the margins of, or outside, current reserves, while the more resilient species retains a greater share of expanding suitable area within or adjacent to protected lands (Figure 7). This spatial mismatch between static protection and dynamic climate niches has been demonstrated in other hotspot assessments and argues strongly for adaptive, forward-looking conservation planning that explicitly integrates future suitability into PA design and management[76,77]. At the same time, model uncertainty is spatially patterned: peripheral lowlands and parts of southern ranges show elevated prediction disagreement, indicating where fine-scale microclimatic heterogeneity and local land-use will be most important to assess via field validation before implementing large-scale interventions[10].

- *Conservation Implications*

Although projected scenarios indicate substantial loss of suitable habitat for *D. floribundus*, the proportion of habitat within protected areas shows minor variations across scenarios, suggesting that current conservation coverage may require reassessment to ensure long-term species persistence. Passive protection alone is unlikely to prevent range contraction; active, targeted interventions will be required. Such projected contractions in climatically suitable areas could also have implications for future extinction risk assessments, as substantial reductions in geographic range may influence evaluations under IUCN Criterion B, which considers extent of occurrence (EOO) and area of occupancy (AOO)[78]. We recommend a tiered, proactive strategy: (1) prioritize in-situ management of high-persistence sites, particularly northern and high-elevation refugia; (2) expand or realign protected-area boundaries to capture projected future suitability and facilitate altitudinal or latitudinal shifts; (3) develop ex-situ conservation and seed banking for vulnerable populations; and (4) consider assisted migration trials where natural dispersal may be insufficient. For *D. szowitsianus*, which shows high persistence and expansion potential, monitoring should focus on genetic connectivity and the ecological consequences of range expansion, including interactions with resident taxa. Although increases in suitable climatic areas may partly offset its currently restricted distribution, a formal reassessment of its IUCN Red List status would require additional data on population size, demographic trends, dispersal capacity, and non-climatic threats. Additionally, fine-scale microrefugial mapping, demographic and dispersal studies, and incorporation of non-climatic threats (land use, overgrazing, invasive species) into vulnerability assessments are essential to refine conservation priorities. These measures align with regional recommendations for dynamic protected-area planning and are integrated *in situ* and *ex situ* conservation in mountain endemics.

- *Deficiency and future improvements of this study*

It is essential to recognize the limitations of our modeling framework. While our Maxent-based projections broadly reflect known distributions, they are climate-centric and do not incorporate demographic processes, biotic interactions, soil or microhabitat variability, or anthropogenic pressures such as land-use change and grazing[24,78,79]. Occurrence data limitations, spatial bias, and uneven sampling may also affect niche estimates[80,81,82], and protected-area coverage

derived from www.protectedplanet.net may be incomplete or outdated, underrepresenting actual conservation areas[83,84]. Consequently, projected range shifts and extinction risk should be interpreted cautiously. Future work combining ensemble modeling, demographic and dispersal data, fine-scale field validation, and updated protected-area mapping would refine predictions and support more effective, species-specific conservation planning[85,86].

In conclusion, the asymmetric fates of *D. floribundus* and *D. szowitsianus* in the Irano-Anatolian biodiversity hotspot illustrate how subtle differences in climatic sensitivity and ecological strategy can produce opposing outcomes under the same regional climate trajectories. This case study complements regional and global evidence that mountain endemics are not a monolithic group: some taxa are predisposed to rapid contraction and refuge dependence, while others possess the traits or opportunity space to persist or expand. For a hotspot that concentrates exceptional endemic richness, these findings underscore the importance of spatially explicit assessments of species' ranges and highlight the need for species-specific vulnerability analyses and adaptive conservation frameworks that anticipate range shifts, safeguard projected refugia, and integrate fine-scale ecological data to distinguish transient expansions from long-term persistence.

Conclusion

Our findings show that closely related endemic species in the Irano-Anatolian biodiversity hotspot may exhibit markedly divergent biogeographical responses to climate change, a phenomenon attributable to differences in thermal sensitivity, precipitation dependence, and ecological niche breadth. Despite their close taxonomic relationship, our models predict opposing ecological strategies and climatic sensitivities for *D. floribundus* and *D. szowitsianus*. *D. floribundus*, constrained by a narrow thermal niche, is projected to undergo substantial range contraction and an upslope shift into high-elevation refugia, consistent with the "escalator to extinction" paradigm for cold-adapted taxa. Conversely, *D. szowitsianus*, characterized by a broader climatic tolerance, is expected to persist across its current distribution while simultaneously colonizing newly suitable habitats. These results illustrate how subtle variations in climatic niche breadth can generate opposing biogeographical trajectories, even among congeners. Beyond their local significance, these contrasting responses underscore the potential for climate change to decouple established species assemblages, reshape community composition, and reorganize biodiversity patterns within montane landscapes. By showing that species within the same genus and biodiversity hotspot can face opposite fates under identical climate scenarios, this study advances a broader understanding of how climate-driven range dynamics operate. Our work thus reinforces the importance of conducting species-specific vulnerability assessments and offers a framework for anticipating the heterogeneous and often unpredictable outcomes of climate change in global biodiversity hotspots.

References

1. Myers, N., Mittermeier, R. A., Mittermeier, C. G., da Fonseca, G. A. B. & Kent, J. Biodiversity hotspots for conservation priorities. *Nature* **403**, 853–858 (2000).

2. Mittermeier, R. A., Turner, W. R., Larsen, F. W., Brooks, T. M. & Gascon, C. Global biodiversity conservation: the critical role of hotspots. In *Biodiversity Hotspots* (eds. Zachos, F. E. & Habel, J. C.) 3–22 (Springer, Berlin, 2011).

3. Brooks, T. M. *et al.* Global biodiversity conservation priorities. *Science* **313**, 58–61 (2006).

4. Noroozi, J. *et al.* Patterns of endemism in Turkey, the meeting point of three global biodiversity hotspots, based on three diverse families of vascular plants. *Front. Ecol. Evol.* **7**, 159 (2019).

5. Özkan, A. M., Koç, M. & Karavelioğulları, F. A. Patterns of endemism in Turkey: the meeting point of three global biodiversity hotspots. *Front. Ecol. Evol.* **7**, 159 (2019).

6. Noroozi, J. *et al.* Endemics determine bioregionalization in the alpine zone of the Irano-Anatolian biodiversity hotspot (South-West Asia). *Alpine Bot.* **131**, 177–186 (2021).

7. Noroozi, J. *et al.* Hotspots within a global biodiversity hotspot—areas of endemism are associated with high mountain ranges. *Sci. Rep.* **8**, 10345 (2018).

8. Lenoir, J. *et al.* A significant upward shift in plant species optimum elevation during the 20th century. *Science* **320**, 1768–1771 (2008).

9. Dullinger, S. *et al.* Post-glacial migration lag restricts range filling of plants in the European Alps. *Glob. Ecol. Biogeogr.* **21**, 829–840 (2012).

10. Pauli, H. *et al.* Recent plant diversity changes on Europe's mountain summits. *Science* **336**, 353–355 (2012).

11. Steinbauer, M. J. *et al.* Accelerated increase in plant species richness on mountain summits is linked to warming. *Nature* **556**, 231–234 (2018).

12. Moradi, H., Noroozi, J. & Fourcade, Y. Plant endemic diversity in the Irano-Anatolian global biodiversity hotspot is dramatically threatened by future climate change. *Biol. Conserv.* **302**, 110963 (2025).

13. Davis, P. H., Mill, R. R. & Tan, K. (eds). *Flora of Turkey and the East Aegean Islands*, Vols. 1–10 (Edinburgh University Press, Edinburgh, 1965–1988).

14. Rechinger, K. H. *Flora Iranica*, No. 163: Caryophyllaceae II (Akademische Druck- und Verlagsanstalt, Graz, 1988).

15. Assadi, M. *et al. Flora of Iran*, No. 168: Caryophyllaceae (Research Institute of Forests and Rangelands, Tehran, 2023).

16. Plants of the World Online. *Dianthus pseudocrinitus*. Royal Botanic Gardens, Kew. Available from: https://powo.science.kew.org (accessed 2026) (2024).

17. Ghahremaninejad, F., Alirezaei, Z., Mohammadi, M. and Nejad Falatoury, A. Updated catalogue of Iran's endemic angiosperms. Taxonomy and Biosystematics, **17(3)**, 23-70 (2025).

18. Davidson, J. *et al.* The geology of Damavand volcano, Alborz Mountains, northern Iran. *Geol. Soc. Am. Bull.* **116**, 16–29 (2004).

19. Sorkhabi, R. B. (ed.). *Tectonic Evolution, Collision, and Seismicity of Southwest Asia: In Honor of Manuel Berberian's Forty-five Years of Research Contributions*, Vol. 525 (Geological Society of America, 2017).

20. Elith, J. & Leathwick, J. R. Species distribution models: ecological explanation and prediction across space and time. *Annu. Rev. Ecol. Evol. Syst.* **40**, 677–697 (2009).

21. Peterson, A. T. *et al. Ecological Niches and Geographic Distributions* (Princeton University Press, Princeton, 2011).

22. Guisan, A., Thuiller, W. & Zimmermann, N. E. *Habitat Suitability and Distribution Models: With Applications in R* (Cambridge University Press, Cambridge, 2017).

23. Phillips, S. J., Anderson, R. P. & Schapire, R. E. Maximum entropy modeling of species geographic distributions. *Ecol. Modell.* **190**, 231–259 (2006).

24. Araújo, M. B. & Peterson, A. T. Uses and misuses of bioclimatic envelope modeling. *Ecology* **93**, 1527–1539 (2012).

25. Babanezhad, R. & Naqinezhad, A. Species distribution modeling of Iranian montane plants under climate change scenarios. *Plant Ecol. Evol.* **157**, 45–58 (2024).

26. Assadi, M. The genus *Dianthus* L. (Caryophyllaceae) in Iran. *Iran. J. Bot.* **3**, 9–54 (1985).

27. Aiello-Lammens, M. E., Boria, R. A., Radosavljevic, A., Vilela, B. & Anderson, R. P. spThin: an R package for spatial thinning of species occurrence records for use in ecological niche models. *Ecography* **38**, 541–545 (2015).

28. Boria, R. A., Olson, L. E., Goodman, S. M. & Anderson, R. P. Spatial filtering to reduce sampling bias can improve the performance of ecological niche models. *Ecol. Modell.* **275**, 73–77 (2014).

29. Varela, D., Romeiras, M. M. & Silva, L. Implications of climate change on the distribution and conservation of Cabo Verde endemic flora. *Ecol. Evol.* **12**, e02025 (2022).

30. Hijmans, R. J. Cross-validation of species distribution models: removing spatial sorting bias and calibration with a null model. *Ecology*, 90(3), 679–688 (2012).

31. Fitzpatrick, M. C., N. J. Gotelli, and A. M. Ellison. MaxEnt versus MaxLike: empirical comparisons with ant species distributions. Ecosphere 4(5):55 (2013).

32. Radosavljevic, A. & Anderson, R. P. Making better Maxent models of species distributions. *J. Biogeogr.* **41**, 629–643 (2014).

33. Cobos, M. E., Peterson, A. T., Barve, N. & Osorio-Olvera, L. kuenm: an R package for detailed development of ecological niche models using Maxent. *PeerJ* **7**, e6281 (2019).

34. Karger, D. N. *et al.* Climatologies at high resolution for the Earth's land surface areas. *Sci. Data* **4**, 170122 (2017).

35. Karger, D. N. *et al.* Climatologies at high resolution for the Earth's land surface areas (CHELSA V2.1). *Sci. Data* **8**, 1–14 (2021).
36. Bauer, N. *et al.* Shared socio-economic pathways of the energy sector—quantifying the narratives. *Glob. Environ. Change* **42**, 316–330 (2017).
37. Tebaldi, C. *et al.* Climate model projections from the Scenario Model Intercomparison Project (ScenarioMIP) of CMIP6. *Earth Syst. Dynam.* **12**, 253–293 (2021).
38. Yates, K. L. *et al.* Outstanding challenges in the transferability of ecological models. *Trends Ecol. Evol.* **33**, 790–802 (2018).
39. Escobar, L. E., Lira-Noriega, A., Medina-Vogel, G. & Peterson, A. T. Potential for spread of the white-nose fungus (*Pseudogymnoascus destructans*) in the Americas: use of Maxent and NicheA to assure strict model transference. *EcoHealth* **11**, 620–631 (2014).
40. Barve, N. *et al.* The crucial role of the accessible area in ecological niche modeling and species distribution modeling. *Ecol. Modell.* **222**, 1810–1819 (2011).
41. Machado-Stredel, F., Cobos, M. E. & Peterson, A. T. A simulation-based method for selecting calibration areas for ecological niche models. *Front. Biogeogr.* **13**, e48814 (2021).
42. Amaro, G. *et al.* Effect of study area extent on the potential distribution of species. *Ecol. Modell.* **483**, 110454 (2023).
43. Morales, N. S., Fernández, I. C., & Baca-González, V. MaxEnt's parameter configuration and small samples: are we paying attention to recommendations? A systematic review. PeerJ, **5**, e3093 (2017).
44. Peterson, A. T., Cobos, M. E. & Jiménez-García, D. Major challenges for correlational ecological niche model projections to future climate conditions. *Ann. N. Y. Acad. Sci.* **1429**, 66–77 (2018).
45. Anderson, R. P., Lew, D. & Peterson, A. T. Evaluating predictive models of species' distributions. *Ecol. Modell.* **162**, 211–232 (2003).
46. Warren, D. L. & Seifert, S. N. Ecological niche modeling in Maxent. *Ecol. Appl.* **21**, 335–342 (2011).
47. Whitford, A. M., Shipley, B. R., & McGuire, J. L. The influence of the number and distribution of background points in presence-background species distribution models. Ecological Modelling, **488**, 110604 (2024).
48. Wenger, S. J. & Olden, J. D. Assessing transferability of ecological models. *Methods Ecol. Evol.* **3**, 260–267 (2012).
49. Peterson, A. T., Papeş, M. & Eaton, M. Transferability and model evaluation in ecological niche modeling. *Ecography* **30**, 550–560 (2007).
50. Hijmans, R. J. terra: spatial data analysis in R. R package version 1.x. (2025).
51. Campbell, L. P. *et al.* Climate change influences on global distributions of dengue and chikungunya virus vectors. *Phil. Trans. R. Soc. B* **370**, 20140135 (2015).
52. R Core Team. R: a language and environment for statistical computing. R Foundation for Statistical Computing (2018).
53. Hijmans, R. J. & Graham, C. H. The ability of climate envelope models to predict the effect of climate change. *Glob. Change Biol.* **12**, 2272–2281 (2006).

54. Hijmans, R. J. *raster: Geographic data analysis and modeling*. R package version 3.6-32 (2025)
55. Hijmans, R. J. *terra: Spatial data analysis*. R package version 1.8-54 (2025)
56. Pebesma, E. Simple features for R: Standardized support for spatial vector data. R J. 10, 439–446 (2018)
57. Wickham, H. *ggplot2: Elegant graphics for data analysis*. Springer, New York (2016)
58. Parmesan, C. Ecological and evolutionary responses to recent climate change. *Annu. Rev. Ecol. Evol. Syst.* **37**, 637–669 (2006).
59. Behroozian, M. *et al.* Climate change influences on the potential distribution of *Dianthus polylepis*. *PLoS ONE* **15**, e0237527 (2020).
60. Atashgahi, Z. *et al.* Endemic cushions of the Khorassan–Kopet Dagh floristic province show differential responses to future climate change. *Sci. Rep.* **15**, 16046 (2025).
61. Alipour, S. & Behroozian, M. Potential impacts of climate change on *Dionysia diapensiifolia*. *J. Nat. Conserv.* **88**, 127050 (2025).
62. Zimmermann, N. E. *et al.* Climatic extremes improve predictions of spatial patterns of tree species. *Proc. Natl Acad. Sci. USA* **106**, 19723–19728 (2009).
63. Dullinger, S. *et al.* Extinction debt of high-mountain plants under twenty-first-century climate change. *Nat. Clim. Change* **2**, 619–622 (2012).
64. Körner, C. *Alpine Plant Life: Functional Plant Ecology of High Mountain Ecosystems* (2nd ed.). Springer (2003).
65. Larcher, W. *Physiological Plant Ecology* (4th ed.). Springer (2003).
66. Nicotra, A. B., Atkin, O. K., Bonser, S. P., Davidson, A. M., Finnegan, E. J., Mathesius, U., ... & Valladares, F. Plant phenotypic plasticity in a changing climate. *Trends in Plant Science*, 15(12), 684–692 (2010).
67. Valladares, F., Matesanz, S., Guilhaumon, F., Araujo, M. B., Balaguer, L., Benito-Garzón, M., ... & Zaragoza-Castells, J. The effects of phenotypic plasticity and local adaptation on forecasts of species range shifts under climate change. *Ecology Letters*, 17(11), 1351–1364 (2014).
68. Reich, P. B. (2014). The world-wide 'fast–slow' plant economics spectrum: A traits manifesto. *Journal of Ecology*, 102(2), 275–301.
69. Dirnböck, T., Essl, F. & Rabitsch, W. Disproportional risk for habitat loss of high-altitude endemic species. *Glob. Change Biol.* **17**, 990–996 (2011).
70. Thuiller, W. *et al.* Climate change threats to plant diversity in Europe. *Proc. Natl Acad. Sci. USA* **102**, 8245–8250 (2005).
71. Karami, S. *et al.* Minimal climate change impacts on *Nepeta glomerulosa*. *Sci. Rep.* **12**, 19893 (2022).
72. Noedoost, F. *et al.* Potential impacts of climate change on *Achillea eriophora*. *Ecol. Evol.* **14**, e11241 (2024).
73. Araújo, M. B. & Luoto, M. The importance of biotic interactions for modelling species distributions. *Glob. Ecol. Biogeogr.* **16**, 743–753 (2007).

74. Svenning, J. C. & Sandel, B. Disequilibrium vegetation dynamics under future climate change. *Am. J. Bot.* **100**, 1266–1286 (2013).
75. Alexander, J. M., Diez, J. M. & Levine, J. M. Novel competitors shape species' responses to climate change. *Nature* **525**, 515–518 (2015).
76. Hannah, L. *et al.* Protected area needs in a changing climate. *Front. Ecol. Environ.* **5**, 131–138 (2007).
77. Watson, J. E. M., Dudley, N., Segan, D. B. & Hockings, M. The performance and potential of protected areas. *Nature* **515**, 67–73 (2014).
78. Wisz, M. S. *et al.* The role of biotic interactions in shaping distributions of species. *Biol. Rev.* **88**, 15–30 (2013).
79. Franklin, J. Species distribution models in conservation biogeography. *Divers. Distrib.* **19**, 1217–1223 (2013).
80. Phillips, S. J. *et al.* Sample selection bias and presence-only distribution models. *Ecol. Appl.* **19**, 181–197 (2009).
81. Kramer-Schadt, S. *et al.* The importance of correcting for sampling bias in MaxEnt models. *Divers. Distrib.* **19**, 1366–1379 (2013).
82. Fourcade, Y., Engler, J. O., Rödder, D. & Secondi, J. Mapping species distributions with Maxent using biased samples. *PLoS ONE* **9**, e97122 (2014).
83. Butchart, S. H. M. *et al.* Shortfalls and solutions for meeting conservation area targets. *Conserv. Lett.* **8**, 329–337 (2015).
84. UNEP-WCMC & IUCN. Protected Planet: the World Database on Protected Areas. (2023).
85. Araújo, M. B. & New, M. Ensemble forecasting of species distributions. *Trends Ecol. Evol.* **22**, 42–47 (2007).
86. Thuiller, W. *et al.* Uncertainty in ensembles of global biodiversity scenarios. *Nat. Commun.* **10**, 1446 (2019).

Acknowledgments

The author would like to thank Mohammad Reza Joharchi in Herbarium of Ferdowsi University of Mashhad (FUMH) and Dr. Mostafa Assadi in Herbarium of Research Institute of Forests and Rangelands (TARI) for providing certain occurrence data.

Contributions

M.B. conceived and designed the study, collected the data, and performed the analyses, and wrote the first version of the draft and revised it.

Data availability

All data supporting the findings of this study are available in the Supplementary Information file.

Competing interests

The author declare no competing interests.

Declarations

The author declare no competing interests.

Funding

No funding

738 **Table 1.** The details of the assessment of area (km^2) and percentage of the potential distribution of *Dianthus*
739 *floribundus* and *Dianthus szowitsianus* in the suitable, unsuitable areas, expansion, contraction, and persistence for
740 the Irano-Anatolian biodiversity hotspot.

		Irano-Anatolian biodiversity hotspot		Irano-Anatolian biodiversity hotspot	
		Dianthus floribundus		*Dianthus szowitsianus*	
		Area (km^2)	percentage of the potential distribution	Area (km^2)	percentage of the potential distribution
Suitable area	current	404222	44.44%	273931	30.12%
	SSP3-7.0 (2041-2070)	405983	44.63%	532818	58.58%
	SSP5-8.5 (2041-2070)	371798	40.88%	494085	54.32%
	SSP3-7.0 (2071-2100)	304526	33.48%	587341	64.57%
	SSP5-8.5 (2071-2100)	209389	23.02%	563538	61.96%
Unsuitable area	current	505358	-	635650	-
	SSP3-7.0 (2041-2070)	499475	-	376763	-
	SSP5-8.5 (2041-2070)	533660	-	415496	-
	SSP3-7.0 (2071-2100)	600932	-	322239	-
	SSP5-8.5 (2071-2100)	696069	-	346042	-
Expansion (Gained)	SSP3-7.0 (2041-2070)	94170	23.2%	280036	52.56%
	SSP5-8.5 (2041-2070)	78990	21.25%	234566	47.47%
	SSP3-7.0 (2071-2100)	71035	23.33%	331468	56.44%
	SSP5-8.5 (2071-2100)	47334	22.61%	304144	53.97%
Contraction (Lost)	SSP3-7.0 (2041-2070)	92409	22.86%	21148	7.72%
	SSP5-8.5 (2041-2070)	111414	27.56%	14412	5.26%
	SSP3-7.0 (2071-2100)	170731	42.24%	18057	6.59%
	SSP5-8.5 (2071-2100)	242168	59.91%	14536	5.31%
Persistence (Stable)	SSP3-7.0 (2041-2070)	311813	77.14%	252782	92.28%
	SSP5-8.5 (2041-2070)	292807	72.44%	259518	94.74%
	SSP3-7.0 (2071-2100)	233491	57.76%	255874	93.41%
	SSP5-8.5 (2071-2100)	162054	40.09%	259394	94.69%

741

742

743

744

745

746

747

748 **Table 2.** Projected centroid and elevation shift of *Dianthus floribundus* and *D. szowitsianus* under future climate
749 scenarios (SSP3-7.0 and SSP5-8.5) for 2041–2070 and 2071–2100 in the Irano-Anatolian biodiversity hotspot.

		Present→SSP3-7.0 (2041-2070)	Present→SSP5-8.5 (2041-2070)	Present→SSP3-7.0 (2071-2100)	Present→SSP5-8.5 (2071-2100)
D. floribundus	Centroid Shift (km)	46.6	55.2	99.6	77.5
	Elevation Shift (m)	63.1	83.0	81.4	118.9
	Δlatitude	0.3	0.3	0.6	0.6
	Δlongitude	-0.4	-0.5	-0.8	-0.4
	Bearing (°)	310.8	308.0	314.3	332.8
D. szowitsianus	Centroid Shift (km)	26.2	37.3	37.9	29.7
	Elevation Shift (m)	2.9	-4.7	25.4	45.4
	Δlatitude	-0.2	-0.1	0.0	0.0
	Δlongitude	-0.1	-0.4	-0.4	-0.3
	Bearing (°)	206.9	251.4	273.3	278.4

750

751 **Table 3:** Projected distribution areas of *Dianthus floribundus* and *D. szowitsianus*, including overlap, within the
752 Irano-Anatolian biodiversity hotspot and its protected areas under future climate scenarios (SSP3-7.0 and SSP5-8.5)
753 for 2041–2070 and 2071–2100.

Future scenarios	value	Area in PA (km^2)	Total area (km^2)	Percentage in PA%
SSP3-7.0 (2041-2070)	Unsuitable	11091.5	197840.4	5.60%
	D. floribundus	4815.4	184053.3	2.61%
	D. szowitsianus	11671.7	308699.0	3.78%
	Overlap	9122.1	227183.0	4.01%
SSP5-8.5 (2041-2070)	Unsuitable	11213.5	226012.4	4.96%
	D. floribundus	4968.4	193798.6	2.56%
	D. szowitsianus	12694.3	315374.5	4.02%
	Overlap	7824.5	182590.1	4.28%
SSP3-7.0 (2071-2100)	Unsuitable	10633.9	204547.5	5.19%
	D. floribundus	3862.9	120244.9	3.21%
	D. szowitsianus	14589.1	404765.6	3.60%
	Overlap	7614.7	188217.7	4.04%
SSP5-8.5 (2071-2100)	Unsuitable	10882.9	242555.2	4.48%
	D. floribundus	3845.3	106395.2	3.61%
	D. szowitsianus	17290.4	463376.2	3.73%
	Overlap	4682.1	105449.1	4.44%

754

755

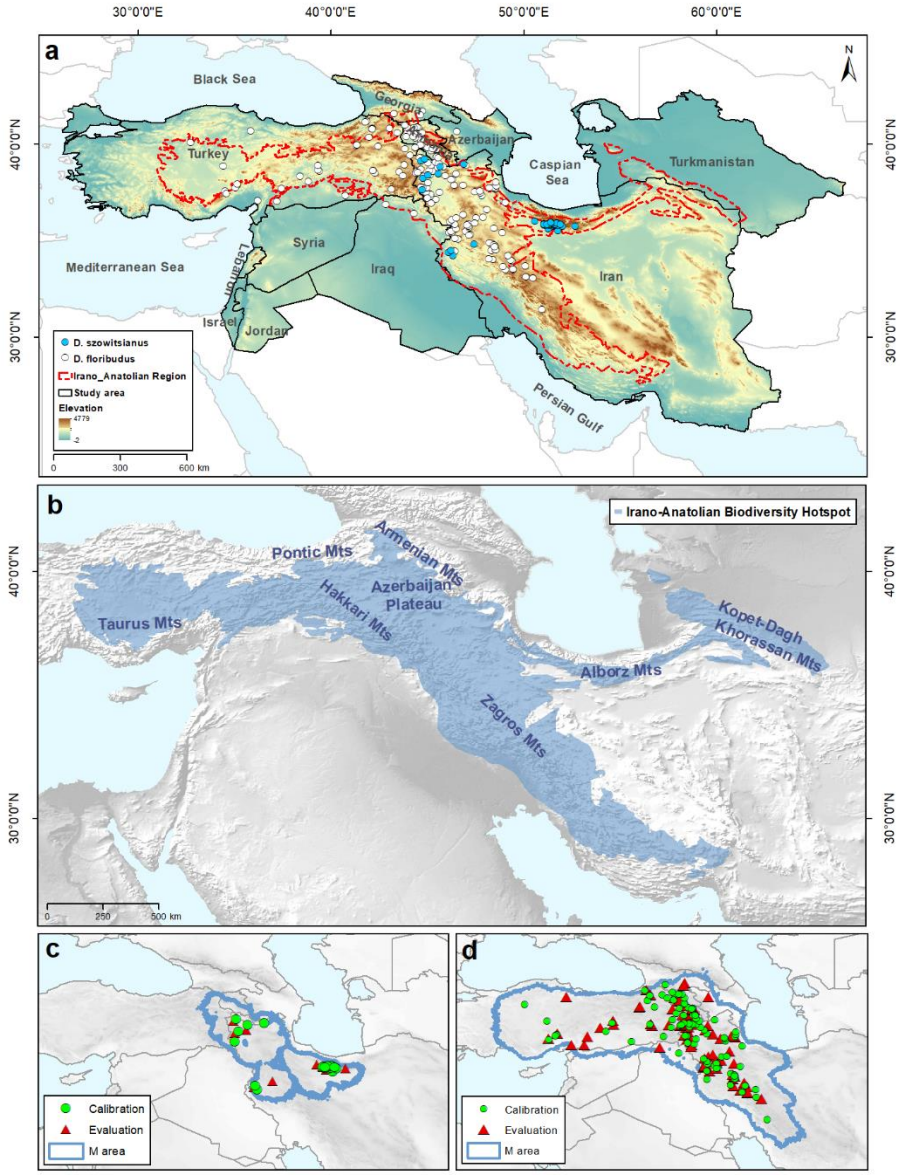

Figure 1. Study area (western Asia and Irano-Anatolian biodiversity hotspot) and distribution of *Dianthus floribundus* and *Dianthus szowitsianus*. **a**) Study area (the countries of western Asia) and occurrence points of *D. floribundus* and *D. szowitsianus* for modeling analysis. **b**) The region of Irano-Anatolian biodiversity hotspot and montane ranges. **c, d**) Occurrence records of *D. szowitsianus* and *D. floribundus*, respectively, in a broader view, with the accessible area (**M**) for model calibration.

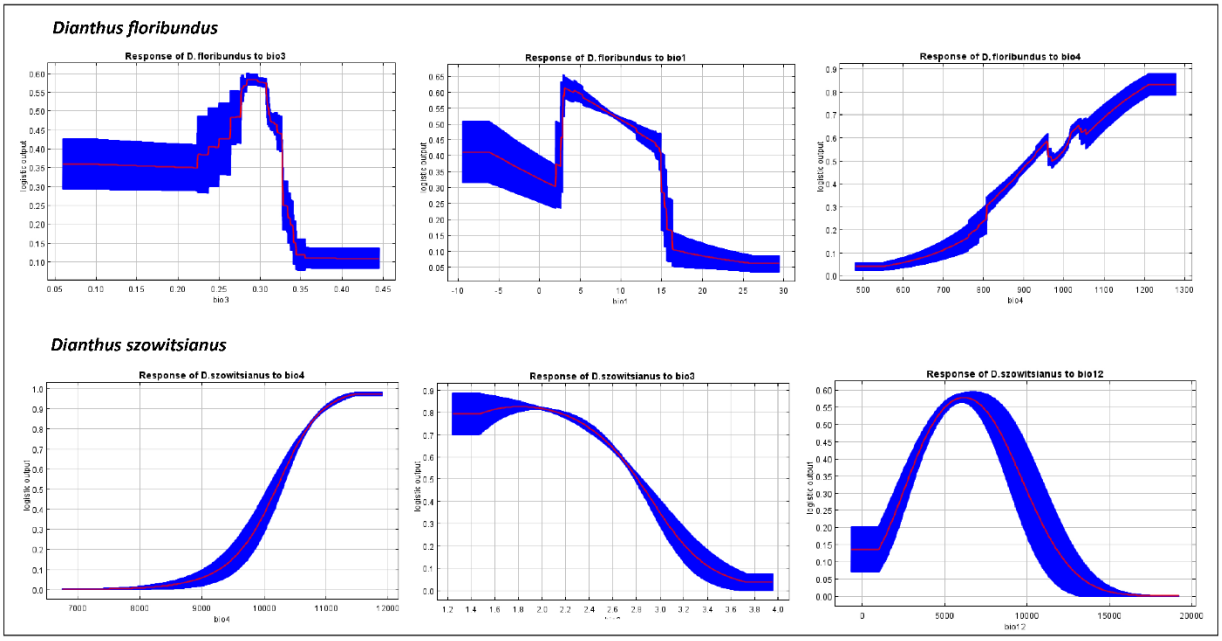

763

764 **Figure 2.** Response curves of the most important bioclimatic predictors for habitat suitability of *Dianthus*
765 *floribundus* and and *D. szowitsianus*

766

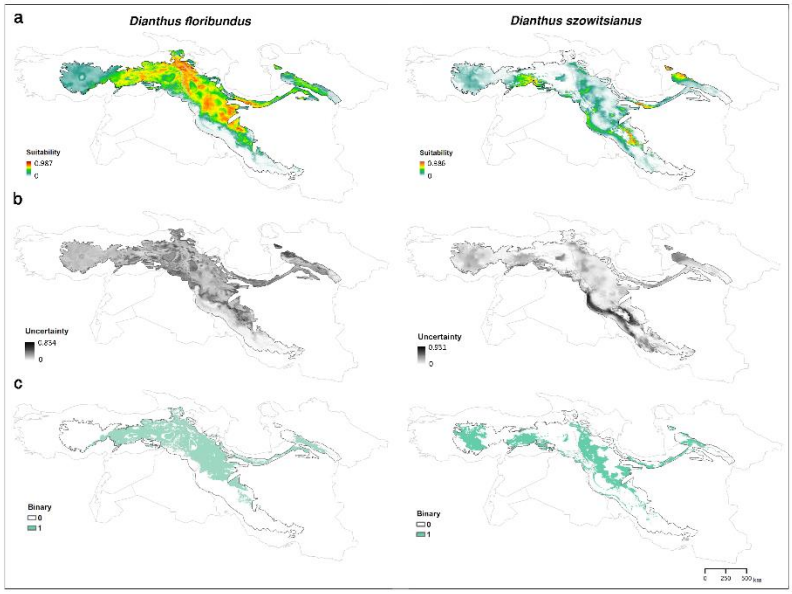

767

768 **Figure 3.** Potentially suitable areas of *Dianthus floribundus* and *D. szowitsianus* based on Maxent model outputs
769 under current conditions in Irano-Anatolian biodiversity hotspot. **a**) The predicted areas of high suitability for the
770 current condition (median prediction). **b**) The uncertainty associated with predictions of suitability under current
771 conditions. **c**) Binary map based on a least training presence thresholding approach.

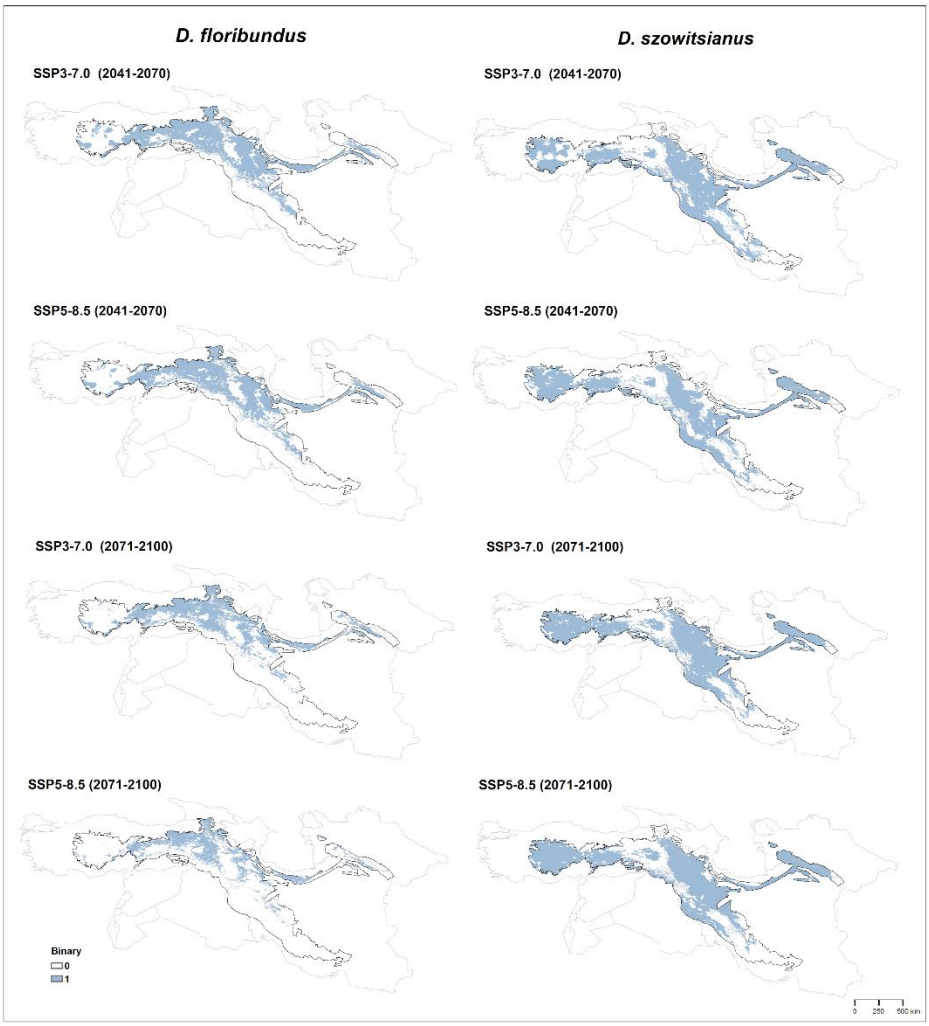

772

773 **Figure 4.** Binary maps based on a least training presence thresholding approach for *Dianthus floribundus* and
774 *Dianthus szowitsianus* under future climate scenarios (SSP3-7.0 and SSP5-8.5) for 2041–2070 and 2071–2100
775 within the protected areas (PA) of the Irano-Anatolian biodiversity hotspot.

776

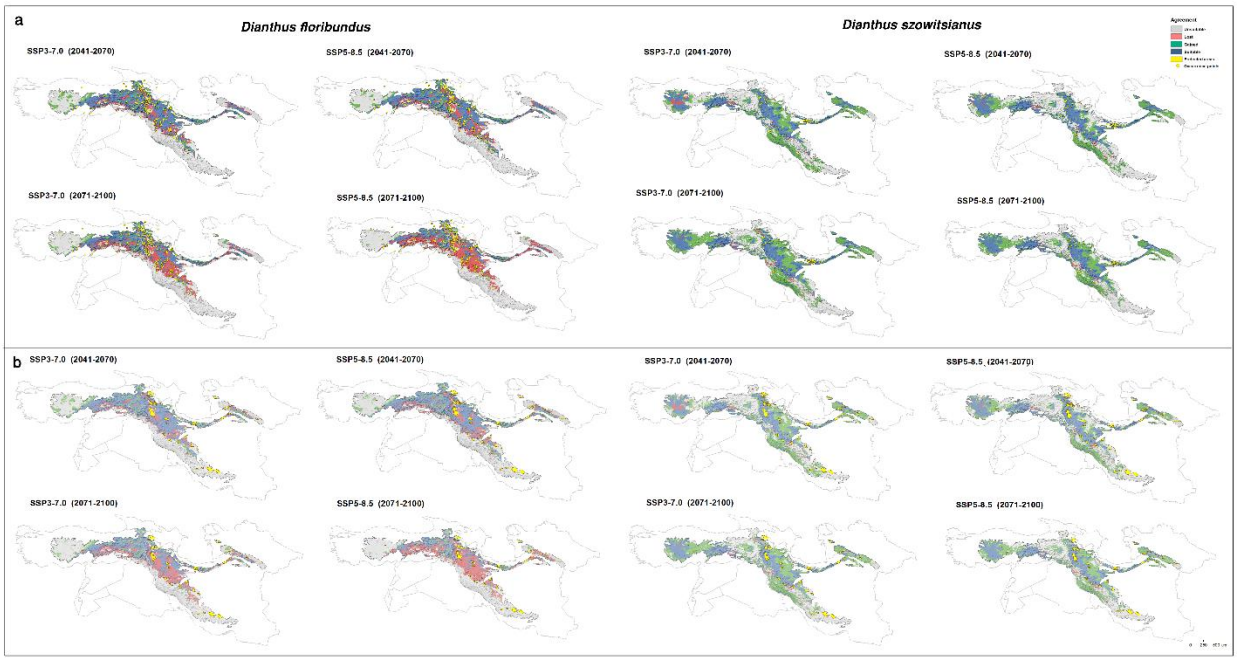

Figure 5. a) Predicted suitable areas and changes in suitability of *Dianthus floribundus* and *D. szowitsianus* based on Maxent model outputs under two climate change scenarios, SSP3-7.5 and SSP5-8.5, for mid-century (2041-2070) and late-century (2071-2100), and agreement between different general circulation models. The occurrence records are represented as yellow points. **b**) Location of protected areas in Irano-Anatolian biodiversity hotspot (yellow polygon). Habitat suitability and contraction areas for both species with regard to the position and extent of protected areas of the Irano-Anatolian biodiversity hotspot.

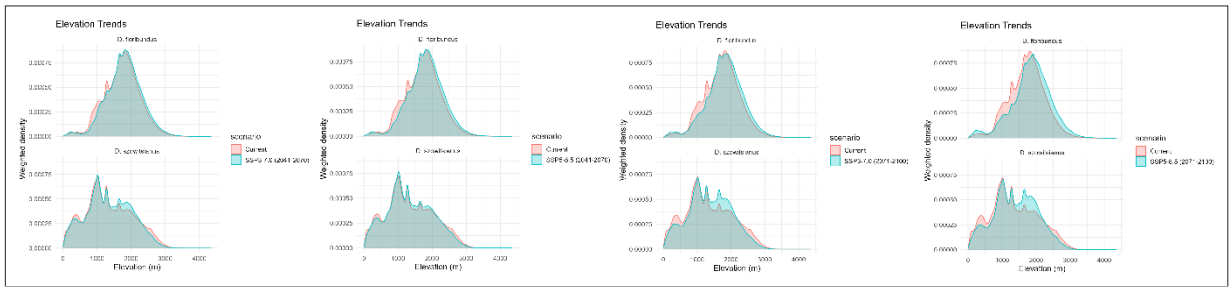

Figure 6. Changes in elevation-weighted habitat suitability of *Dianthus floribundus* and *D. szowitsianus* under current conditions and future climate scenarios (SSP3-7.0 and SSP5-8.5) for mid-century (2041–2070) and late-century (2071–2100).

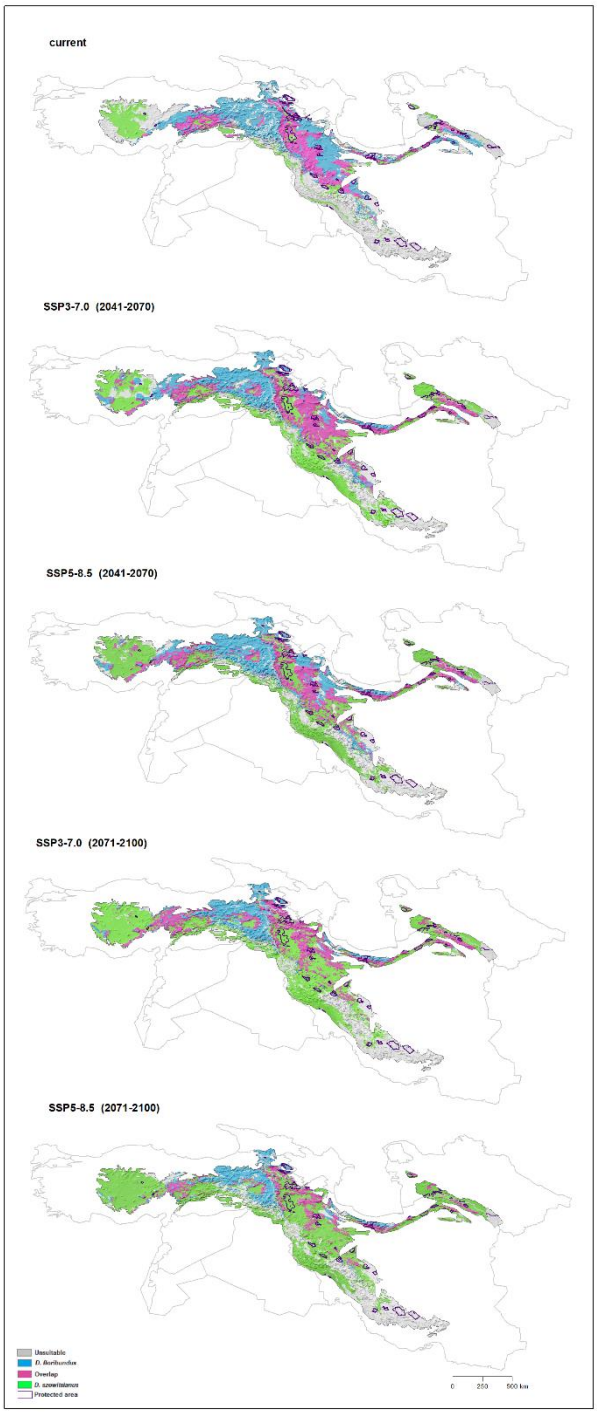

792

793 **Figure 7.** Predicted spatial overlap of *Dianthus floribundus* and *D. szowitsianus* distributions under current and
794 future climate scenarios (SSP3-7.0 and SSP5-8.5) for mid-century (2041–2070) and late-century (2071–2100), in
795 relation to protected areas of the Irano-Anatolian biodiversity hotspot.

796

797

Supplementary

Table S1. A list of models used for SSP3-7.5 and SSP5-8.5 scenarios.

No.	Model name	Abbreviation name
1	National Oceanic and Atmospheric Administration, Geophysical Fluid Dynamics Laboratory, Princeton, NJ 08540, USA	GFDL-ESM4
2	Institute Pierre Simon Laplace, Paris 75252, France	IPSL-CM6A-LR
3	Max Planck Institute for Meteorology, Hamburg 20146, Germany	MPI-ESM1-2-HR
4	the United Kingdom Earth System Model version 1.0, UK	UKESM1-0-LL

Table S2. Variable Importance in Projection (VIP) scores of bioclimatic variables for Dianthus species, calcuated by Partial Least Squares (PLS) regression.

Dianthus szowitsianus		*Dianthus floribundus*	
Variable	VIP_Score	Variable	VIP_Score
ID	1.988148	ID	2.461459
bio4	1.504652	bio6	1.250815
bio3	1.382484	bio11	1.212224
bio7	1.066829	bio1	1.041654
bio2	0.978999	bio4	1.026654
bio14	0.900299	bio7	0.928159
bio12	0.880485	bio10	0.818488
bio17	0.863063	bio3	0.806292
bio6	0.738856	bio5	0.676718
bio15	0.707759	bio12	0.66421
bio13	0.696924	bio13	0.596022
bio5	0.694505	bio2	0.578232
bio16	0.693172	bio14	0.528997
bio11	0.648505	bio16	0.527983
bio10	0.535174	bio17	0.515354
bio1	0.492408	bio15	0.416786

Table S3. Percentage contribution (PC) and permutation importance (PI) of the bioclimatic variables for *Dianthus floribundus* and *Dianthus szowitsianus.*

Bioclimatic variables	Description	PC	PI
Dianthus floribundus			
bio1	Annual Mean Temperature	30.2	18.6
bio4	Temperature Seasonality	26.7	29.6
bio3	Isothermality	26.3	7.6
bio15	Precipitation Seasonality	7.8	14.3
bio13	Precipitation of Wettest Month	5.3	10.5
bio14	Precipitation of Driest Month	3.7	19.5
Dianthus szowitsianus			
bio4	Temperature Seasonality	40.3	47.8
bio3	Isothermality	25.9	1.5
bio12	Annual Precipitation	21	17.7
bio15	Precipitation Seasonality	8.2	9.7
bio7	Temperature Annual Range	4.5	23.3

Table S4. Summary of model parameter settings explored and tested in this study for *Dianthus floribundus* and *Dianthus szowitsianus* (excel file).

Table S5. Projected habitat stability, loss, gain, and absence for *Dianthus floribundus* and *Dianthus szowitsianus* under future climate scenarios (SSP3-7.0 and SSP5-8.5) for 2041–2070 and 2071–2100 within the protected areas (PA) of the Irano-Anatolian biodiversity hotspot.

		Irano-Anatolian biodiversity hotspot		**Irano-Anatolian biodiversity hotspot**	
		Dianthus floribundus		***Dianthus szowitsianus***	
		Protected area (PA) (km^2)	percentage of potential distribution in PA%	Protected area (PA) (km^2)	percentage of potential distribution in PA%
No habitat	SSP3-7.0 (2041-2070)	16997.3649	46.12%	15206.4928	41.26%
	SSP5-8.5 (2041-2070)	17244.6087	46.79%	16057.0936	43.57%
	SSP3-7.0 (2071-2100)	17334.6227	47.04%	14467.965	39.26%
	SSP5-8.5 (2071-2100)	17690.1197	48.00%	14472.0172	39.27%
Lost in the future	SSP3-7.0 (2041-2070)	5835.98874	15.84%	778.387154	2.11%
	SSP5-8.5 (2041-2070)	6743.73172	18.30%	213.540869	0.58%
	SSP3-7.0 (2071-2100)	8028.79136	21.79%	103.243722	0.28%
	SSP5-8.5 (2071-2100)	10567.1079	28.67%	319.500123	0.87%
Gained in the future	SSP3-7.0 (2041-2070)	3722.16762	10.10%	7541.70565	20.46%
	SSP5-8.5 (2041-2070)	3474.9238	9.43%	6691.1049	18.16%
	SSP3-7.0 (2071-2100)	3384.90985	9.18%	8280.23346	22.47%
	SSP5-8.5 (2071-2100)	3029.41284	8.22%	8276.1813	22.46%
Stable	SSP3-7.0 (2041-2070)	10297.2201	27.94%	13326.1558	36.16%
	SSP5-8.5 (2041-2070)	9389.47714	25.48%	13891.0021	37.69%
	SSP3-7.0 (2071-2100)	8104.4175	21.99%5	14001.2992	37.99%
	SSP5-8.5 (2071-2100)	5566.10098	15.10%	13785.0428	37.41%

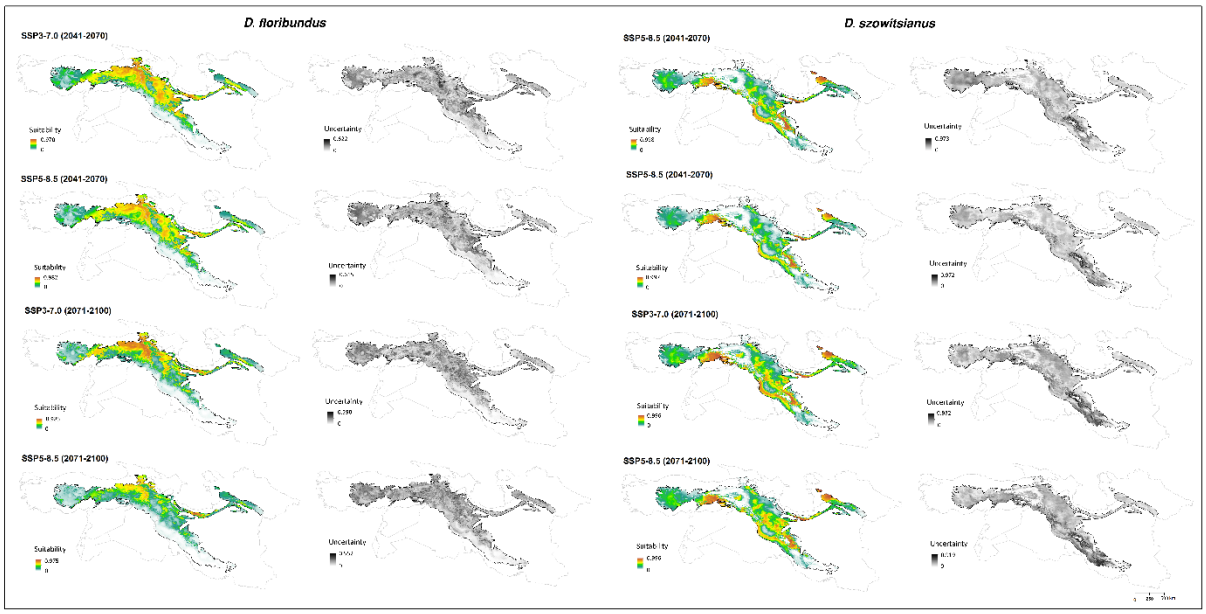

869

870 **Figure S1.** Potential suitable areas of *Dianthus floribundus* and *D. szowitsianus* based on Maxent model outputs
871 under the future (SSP3-7.0 and SSP5-8.5 scenarios) conditions for mid-century (2041-2070) and late-century (2071-
872 2100). Left maps) Predicted areas of high suitability for future conditions (median prediction). Right maps) The
873 uncertainty associated with predictions of suitability under future conditions.

874

875

876

877

878

879

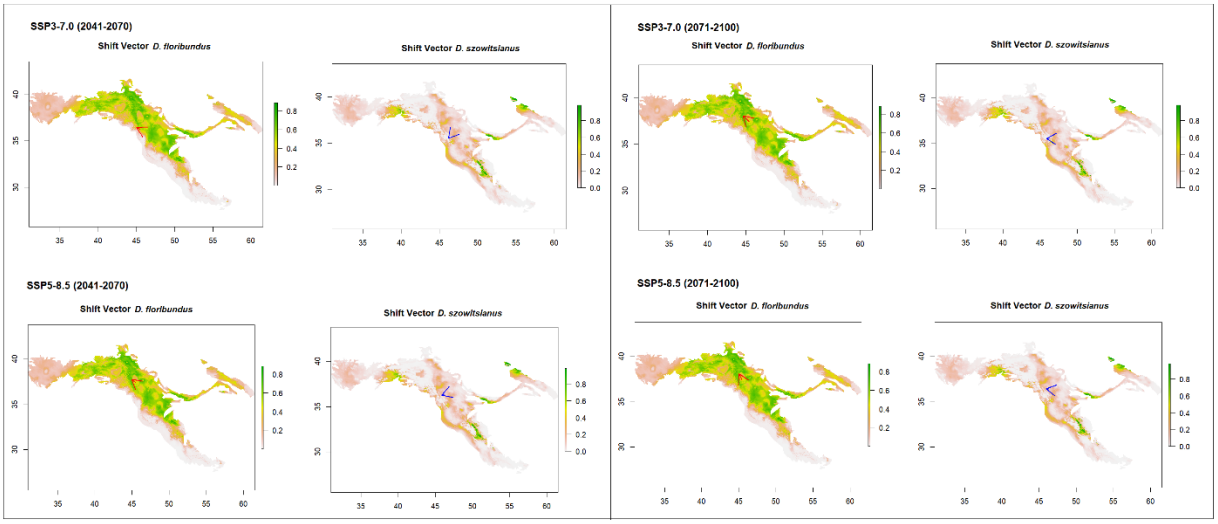

Figure S2. Shift vectors of habitat centroids for *Dianthus floribundus* and *D. szowitsianus* under future climate scenarios (SSP3-7.0 and SSP5-8.5) for mid-century (2041–2070) and late-century (2071–2100).

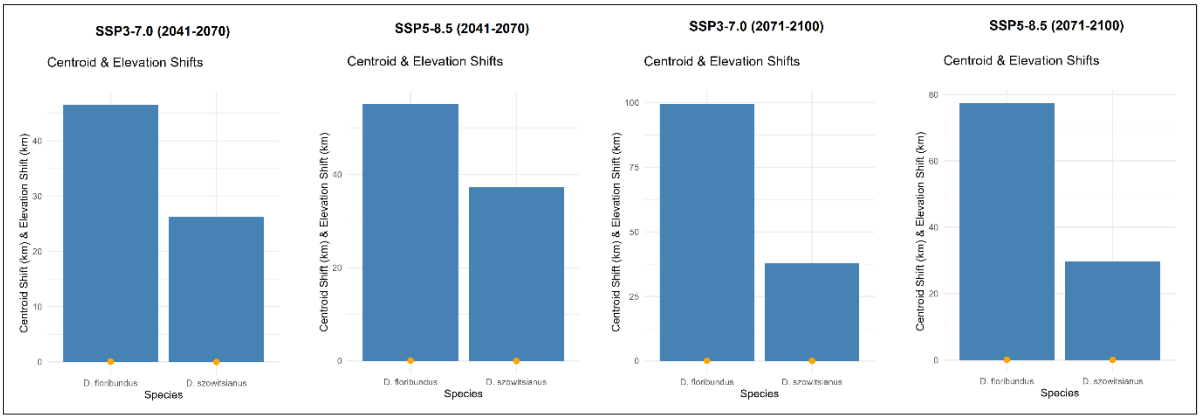

Figure S3. Centroid and elevational shifts of suitable habitats for *Dianthus floribundus* and *D. szowitsianus* under different climate change scenarios (SSP3-7.0 and SSP5-8.5) for mid-century (2041–2070) and late-century (2071–2100).